Hydrogen Generation from Methanol at Near-Room Temperature

Yangbin Shen,[1,2] Yulu Zhan,[1] Shuping Li, [1] Fandi Ning, [1] Ying Du, [1] Yunjie Huang,[3] Ting He[1] and Xiaochun Zhou*,[1,4]

[1] Division of Advanced Nanomaterials, Suzhou Institute of Nano-tech and Nano-bionics, Chinese Academy of Sciences, Suzhou 215125, China

[2] University of Chinese Academy of Sciences, Beijing 100049, China

[3] Faculty of Materials Science and Chemistry, China University of Geosciences, Wuhan 430074, China

[4] Key Laboratory of Nanodevices and Applications, Chinese Academy of Sciences, Suzhou 215125, China

Correspondence and requests for materials should be addressed to X. Z.

Email: xczhou2013@sinano.ac.cn

Table of Contents

SI-1. Chemicals and Materials

All chemicals were commercial and used without further purification unless specified. Ethanol (C_2H_5OH, Tianjing Baishi Chemical Industry Co., Ltd, >99.7%), sodium hydroxide (NaOH, Sinopharm Chemical Reagent, Co., Ltd, >96%), 1,2,3,4,5-pentamethylcyclopentadiene ($C_{10}H_{16}$, Sun Chemical Technology(Shanghai) Co., Ltd, 97%), formic acid (HCOOH, Sinopharm Chemical Reagent. Co., Ltd. >98%), pyrrole (C_4H_5N, Shanghai Macklin Biochemical Co., Ltd., >99%), methanol (CH_3OH, Sinopharm Chemical Reagent, Co., Ltd, >99.7%), chloroiridic acid ($H_2IrCl_6 \cdot 6H_2O$, Shanghai Tuosi Chemical Co., Ltd, Ir wt%>35%), 1,10-phenanthroline ($C_{12}H_8N_2$, Sinopharm Chemical Reagent, Co., Ltd, >99%), iron(III) chloride ($FeCl_3$, Shanghai Macklin Biochemical Co., Ltd. >99.9%), rhodium(III) chloride trihydrate ($RhCl_3$, Adamas Reagent, Ltd.98%), potassium carbonate (K_2CO_3, Sun Chemical Technology(Shanghai) Co., Ltd, 99%), β-Nicotinamide adenine dinucleotide hydrate(NAD^+, Sigma-Aldrich Co. LLC.,≥98%), β-Nicotinamide adenine dinucleotide, reduced disodium salt hydrate(NADH, J&K Scientific Ltd,98%), 1,10-phenanthrolin-5-amine ($C_{12}H_9N_3$,Shanghai Dibo Chemical Reagent, Co., Ltd, ≥97%), N,N-dimethylformamide (DMF, C_3H_7NO, Sinopharm Chemical Reagent, Co., Ltd, >99.5%), 5-nitro-1,10-phenanthroline ($C_{12}H_7N_3O_2$, Meryer (Shanghai) Chemical Technology Co., Ltd.), diethyl ether ($C_4H_{10}O$, Sinopharm Chemical Reagent, Co., Ltd, >99.5%), 2,2'-bipyrimidyl($C_8H_6N_4$, China Langchem Co. Ltd,>98%), ultrapure water was prepared by Thermo PureLab Ultra Genetic.

Enzymes: alcohol dehydrogenase from Saccharomyces cerevisiae (ADH 369 units/mg solid, 383 units/mg protein, molecular weight of ADH (M_{ADH}) =141 kDa, Sigma-Aldrich Co. LLC.), aldehyde dehydrogenase, potassium-activated from baker's yeast (s. cerevisiae) (ALDH 1.8 units/mg solid, 22 units/mg protein, molecular weight of ALDH (M_{ALDH}) =170 kDa, contains lactose, potassium phosphate and citrate buffer salts, and mercaptosuccinic acid, Sigma-Aldrich Co. LLC.).

SI-2. Characterization and physical measurements

^1H NMR spectra of catalysts were recorded on Varian Plus 400 MHz. Gas chromatography experiments were performed on GC-G5 chromatograph with FID/TCD and methanizer (Beijing Persee General Instrument Co., Ltd). The system uses N_2 as a carrier gas, allows for the detection limits of the following gases: H_2≥100 ppm, CO ≥ 1 ppm. The scanning electron microscope images (SEM) were recorded on Quanta 400 FEG, FEI. Thermogravimetric analysis measurement was conducted by TG 209F1 (NETZSCH, Germany), air as carrier gas, gas flow rate is 20 mL min^{-1}, heating rate is 10 K min^{-1}.

UV-absorption and enzymatic reaction kinetics were record by Shimadzu UV-1800. The elemental analysis of C, H and N was performed on Flash 2000 (Thermo Fisher, USA).

SI-3. Preparation of Catalysts

Synthesis of Polypyrrole. The polypyrrole was prepared by chemical polymerization in $FeCl_3$ methanol solution at 10 ℃.[1] The molar ratio of $FeCl_3$ to pyrrole was 2.33:1. The ppy was washed by ultrapure water and dried at room temperature ready for further use.

Synthesis of $[IrCp^*(Cl)_2]_2$. Excess 1,2,3,4,5-pentamethylcyclopentadiene was added in H_2IrCl_6 methanol solution. The molar ratio of 1,2,3,4,5-pentamethylcyclopentadiene to H_2IrCl_6 was about 2.5:1. The mixture was stirred under reflux for 37 h, then cooled to 0 ℃. The yellow brown product will be gained after filtration and washed with ether.[2] (Yield: 70% based on H_2IrCl_6).

Synthesis of Cp^*IrCl_2(ppy). The ppy suspension in excess K_2CO_3 DMF was stirred for 2 h at 55 ℃. Then $[Ir(Cp^*)(Cl)_2]_2$ was added into the suspension, and was kept stirring overnight. The molar ratio of ppy (based on pyrrole monomer) to $[Ir(Cp^*)(Cl)_2]_2$ was 80. The product Cp^*IrCl_2(ppy) was gained after filtration, washed by ultrapure water and dried at room temperature. The Cp^*IrCl_2(ppy) was the novel polymer complex catalyst for HCOOH dehydrogenation. The total process for synthesizing the Cp^*IrCl_2(ppy) was illustrated in **Scheme 2.** (Yield: 68% based on $[IrCp^*(Cl)_2]_2$).

Synthesis of $[RhCp^*(Cl)_2]_2$. 5g rhodium(III) chloride trihydrate, 4 mL pentamethylcyclopentadiene, 100 mL methanol and a magnetic stirring bar were placed in a 250 mL round-bottom flask fitted with a reflux condenser, then the mixture solution refluxed gently under nitrogen for 48h with stirring. During the reaction, the dark red precipitate formed. The product would be filtered off through a glass sinter after the suspension cooled to 0 ℃, then washed with diethyl ether.[3] (Yield: 79% based on $RhCl_3$).

Synthesis of [Cp*IrCl(bpym)]Cl. The $[Ir(Cp^*)(Cl)_2]_2$ reacted with 2 equiv. of 2,2'-bipyrimidine (bpym) in methanol. During the reaction, the $[Ir(Cp^*)(Cl)_2]_2$ would dissolved in methanol gradually, and form the organ-red solution. The yellow product would be gained after removing the methanol by a rotary evaporator, then washed with diethyl ether.[4] (Yield: 90% based on $[IrCp^*(Cl)_2]_2$). Elemental analysis calc. for [Cp*IrCl(bpym)]Cl %C: 38.8, %H: 3.77,%N: 10.06; found %C: 38.41, %H: 3.84, %N: 10.01.

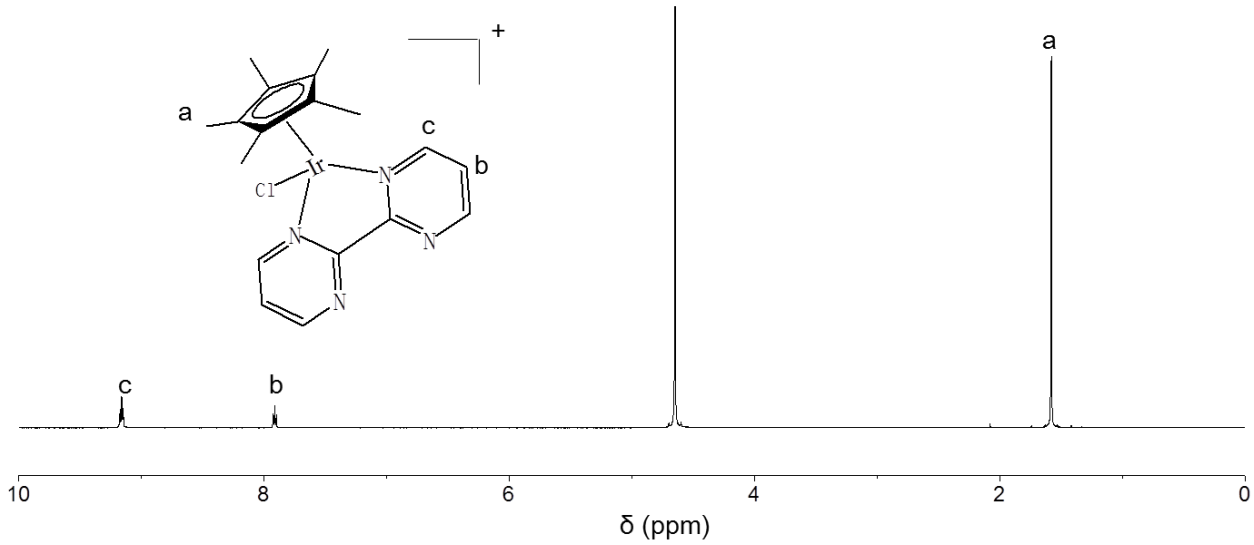

Figure S1. ^{1}H-NMR spectrums of the [Cp*IrCl(bpym)]Cl. ^{1}H NMR (D_2O, 400 MHz) δ_H: 1.55 (15H, s), 7.88 (2H, m), 9.13 (4H, dd).

Synthesis of [Cp*IrCl(phen)]Cl. 2 equiv. of 1,10-phenanthroline was added to a dichloromethane suspension containing $[Ir(Cp^*)(Cl)_2]_2$ for 4 hours. During the reaction, the $[Ir(Cp^*)(Cl)_2]_2$ would dissolved in methanol gradually and the suspension turned into a yellow colour solution. The yellow pure production would be gained after the solution concentrated to dryness and washed by acetone.[5, 6](Yield: 86% based on $[IrCp^*(Cl)_2]_2$). Elemental analysis calc. for [Cp*IrCl(phen)]Cl %C: 45.6, %H: 3.98,%N: 4.84; found %C: 45.41, %H: 4.13, %N: 4.67.

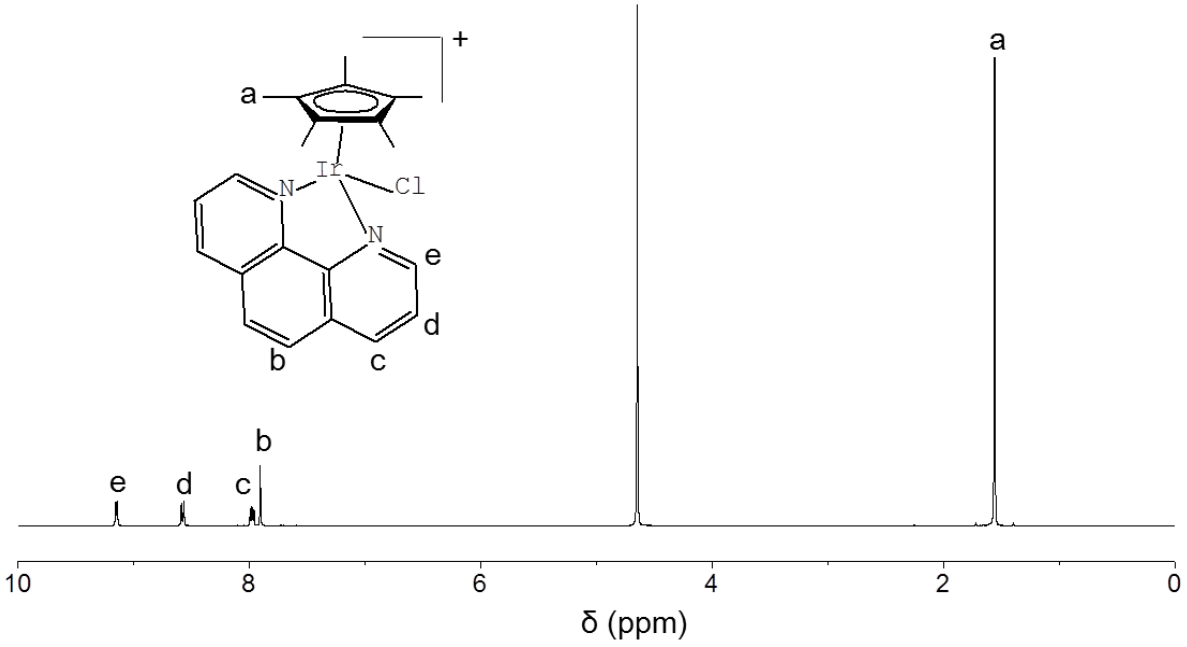

Figure S2. ^{1}H-NMR spectrums of the [Cp*IrCl(phen)]Cl. ^{1}H NMR (D_2O, 400 MHz) δ_H: 1.62 (15H, s), 7.63 (2H, s), 7.96 (2H, d), 8.66 (2H, d), 9.18 (2H, d).

Synthesis of [Cp*IrCl(phen-NH2)]Cl. The $[Ir(Cp^*)(Cl)_2]_2$ reacted with 2 equiv. of 1,10-phenanthrolin-5-amine in dichloromethane. During the reaction, the $[Ir(Cp^*)(Cl)_2]_2$ would dissolved in dichloromethane gradually, and formed the yellow solution. The yellow product would be gained after concentration to dryness by a rotary evaporator, then washed with acetone and yielded a pure yellow powder.[7](Yield: 83% based on $[IrCp^*(Cl)_2]_2$). Elemental analysis calc. for $[Cp^*IrCl(phen\text{-}NH_2)]Cl$ %C: 44.48, %H: 4.04,%N: 7.08; found %C: 44.25, %H: 4.17, %N: 7.20.

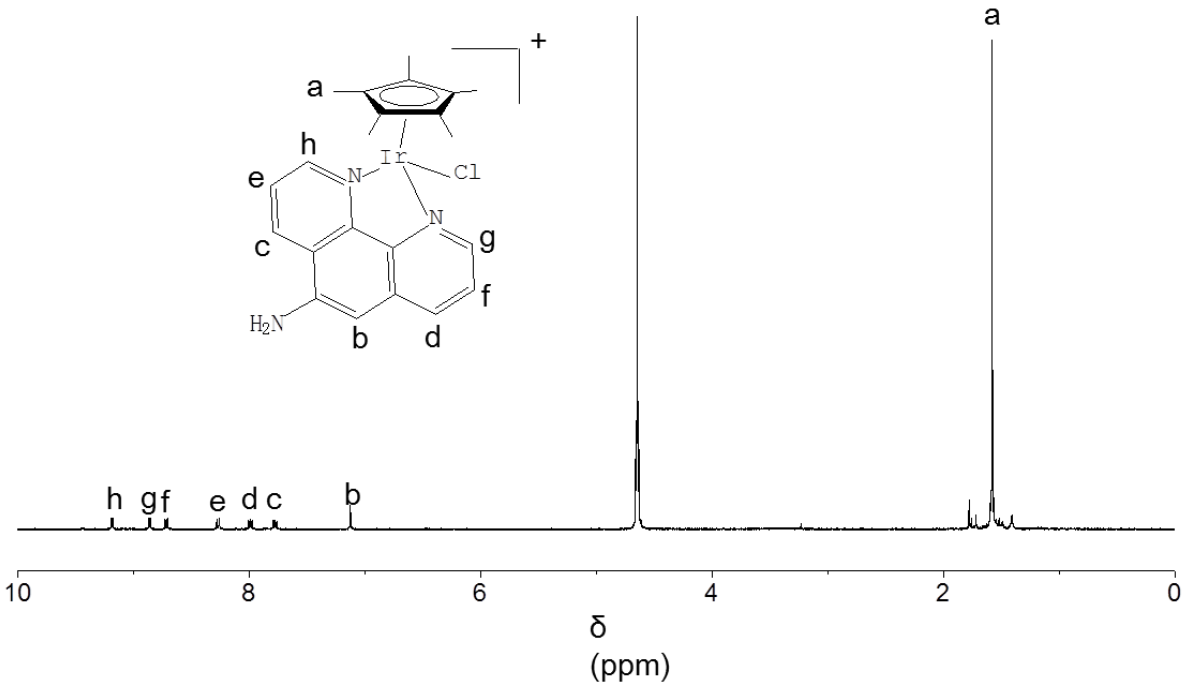

Figure S3. ^{1}H-NMR spectrums of the $[Cp^*IrCl(phen\text{-}NH_2)]Cl$. ^{1}H NMR ($D_2O$, 400 MHz) δ_H: 1.62 (15H, s), 7.13 (1H, s), 7.78 (1H,d), 7.89 (1H, dd), 8.27(1H,d),8.79(1H, d),8.96 (1H, d), 9.18 (1H, d).

Synthesis of [Cp*IrCl(phen-NO$_2$)]Cl. 2 equiv. of the 5-nitro-1,10-phenanthroline were added to a suspension of [Ir(Cp*)(Cl)$_2$]$_2$ in dichloromethane. The mixture was stirred for 3 hours at room temperature, while the colour changed from orange to yellow. After concentration to dryness with the help of the rotary evaporation apparatus, the residue was washed by acetone, which gave a yellow pure product in good yield.[7](Yield: 84% based on [IrCp*(Cl)$_2$]$_2$). Elemental analysis calc. for [Cp*IrCl(phen-NO$_2$)]Cl %C: 42.38, %H: 3.56,%N: 6.74; found %C: 42.41, %H: 3.67, %N: 6.67.

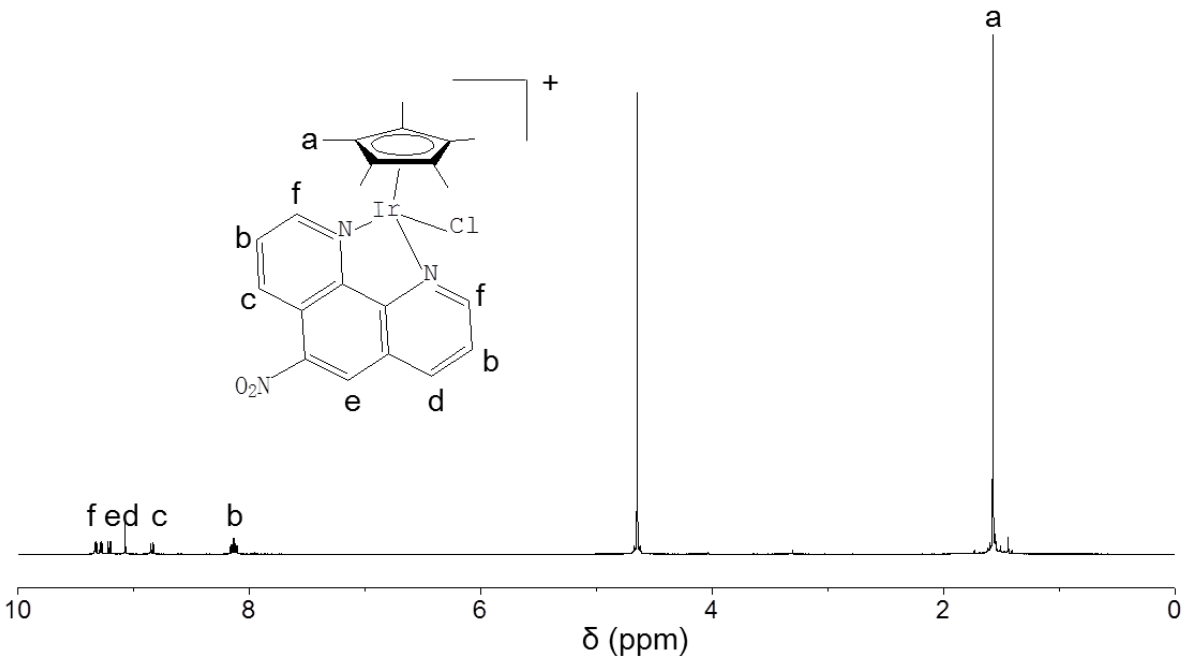

Figure S4. ^{1}H-NMR spectrums of the [Cp*IrCl(phen-NO$_2$)]Cl. ^{1}H NMR (D$_2$O, 400 MHz)δ_H: 1.56 (15H, s), 8.11 (2H, dd) , 8.84 (1H, d), 9.07 (1H, s) ,9.21 (1H, s), 9.30 (2H, dd).

Synthesis of [{Ir(Cp*)(Cl)}$_2$(bpym)]Cl$_2$: This catalyst was prepared by stirring a 1:1 mixture of [IrCp*Cl$_2$]$_2$ and 2,2'-bipyrimidine in methanol for 4 hours. During the reaction, the [Ir(Cp*)(Cl)$_2$]$_2$ would dissolved in methanol gradually, accompanied by red solution formed. The red product would be gained after the methanol removed by the rotary evaporation apparatus.[4,8] The product should be washed with diethyl ether before using. (Yield: 81% based on [IrCp*(Cl)$_2$]$_2$). Elemental analysis calc. for [{Ir(Cp*)(Cl)}$_2$(bpym)]Cl$_2$ %C: 35.18, %H: 3.77,%N: 5.86; found %C: 34.98, %H: 3.63, %N: 5.77.

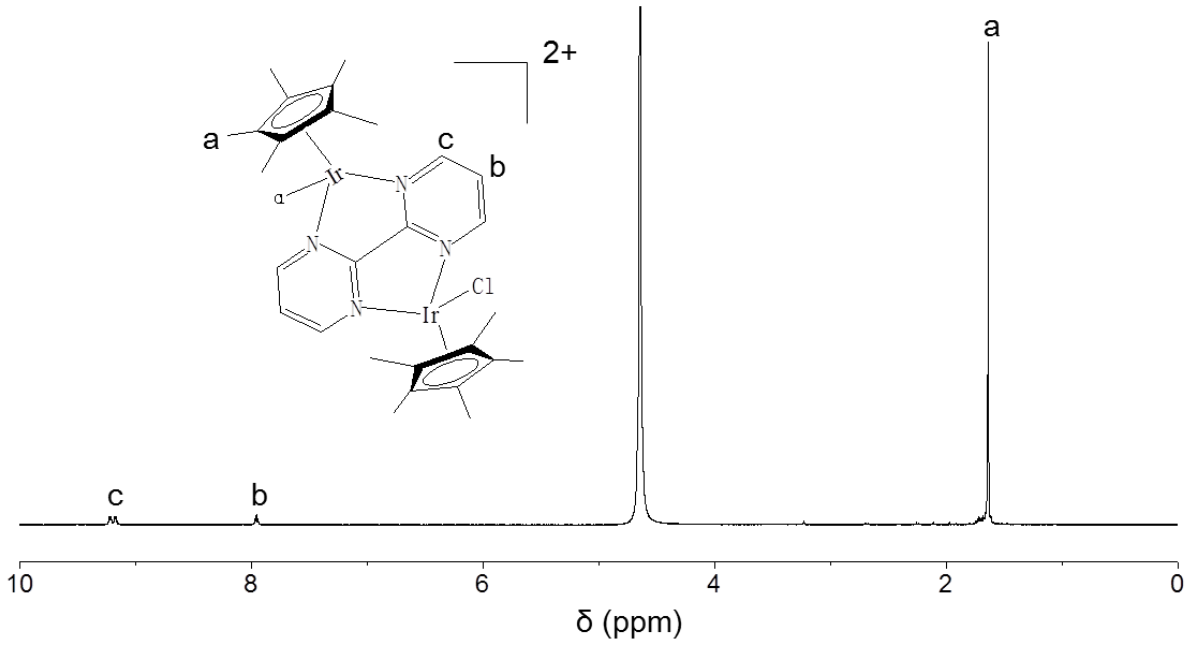

Figure S5. ^{1}H-NMR spectrums of [{Ir(Cp*)(Cl)}$_2$(bpym)]Cl$_2$. ^{1}H NMR (D$_2$O, 400 MHz) δ_H: 1.55 (30H, s), 7.88 (2H, m), 9.13 (4H, dd).

Synthesis of [Cp*RhCl(bpym)]Cl. The $[Rh(Cp^*)(Cl)_2]_2$ reacted with 2 equiv. of 2,2'-bipyrimidine (bpym) in methanol. During the reaction, the $[Rh(Cp^*)(Cl)_2]_2$ would dissolve in methanol gradually, and form the orange solution. After concentration to dryness by a rotary evaporator, a pure yellow powder would be gained.[4] (Yield: 82% based on $[RhCp^*(Cl)_2]_2$). Elemental analysis calc. for $[Cp^*RhCl(bpym)]Cl$ %C: 46.24, %H: 4.49,%N: 11.99; found %C: 46.13, %H: 4.55, %N: 11.27.

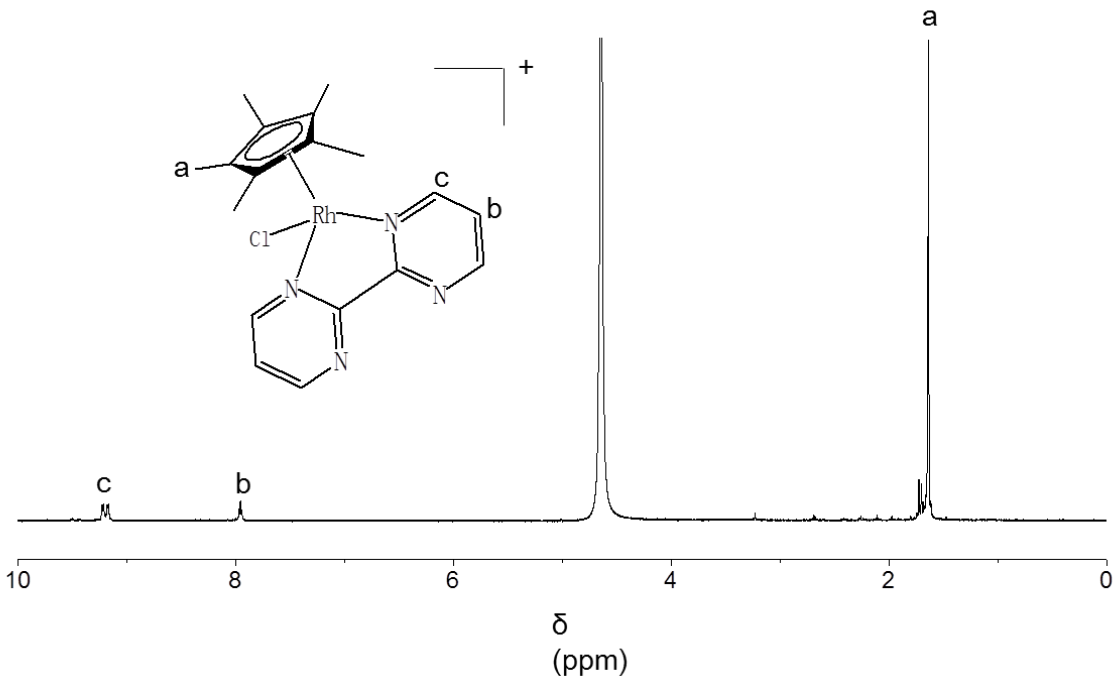

Figure S6. ^{1}H-NMR spectrums of the $[Cp^*RhCl(bpym)]Cl$. ^{1}H NMR (D_2O, 400 MHz) δ_H: 1.61 (15H, s), 7.96 (2H, m), 9.20 (4H, m).

Synthesis of [Cp*RhCl(phen-NO_2)]Cl. The $[Rh(Cp^*)(Cl)_2]_2$ reacted with 2 equiv. of 5-nitro-1,10-phenanthroline in dichloromethane. During the reaction, the $[Rh(Cp^*)(Cl)_2]_2$ would dissolved in dichloromethane gradually, and form the yellow solution. The yellow product would be gained after concentration to dryness by a rotary evaporator, then washed with acetone and yield a pure yellow powder.[7] (Yield: 83% based on $[RhCp^*(Cl)_2]_2$). Elemental analysis calc. for [Cp*RhCl(phen-NO_2)]Cl %C: 49.43, %H: 4.11,%N: 7.87; found %C: 49.31, %H: 4.37, %N: 7.65.

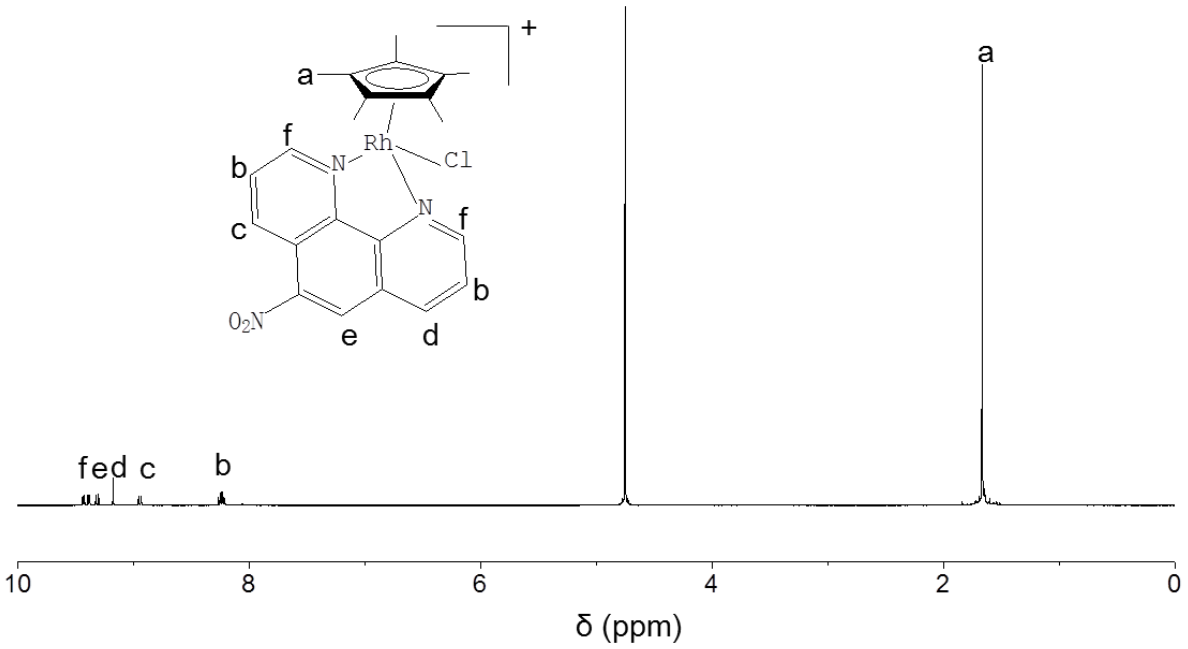

Figure S7. ^{1}H-NMR spectrums of the [Cp*RhCl(phen-NO_2)]Cl. ^{1}H NMR (D_2O, 400 MHz),δ_H: 1.69 (15H, s), 8.10 (2H, dd) , 8.86 (1H, d), 9.09 (1H, s) ,9.23 (1H, s), 9.32 (2H, dd).

SI-4. Experiment for hydrogen generation from methanol

Representative experiment: 0.5 U ALDH, 30 U ADH and 4 mg Catalyst-1 were added in a 25 mL flask which had contained 5 mL phosphate buffer (pH=8.05), 1 mM NAD^+, 500 μM [$Cp^*IrCl(phen)$]Cl. The flask was connected to a u-tube containing colored solution. Then the nitrogen was blow into the total device for more than 10 minutes, replaced the air inside. At last, the methanol was injected into the solution after the flask is heated to preset temperature. The gas content was analyzed by the GC every hour. The activity unit for ADH and ALDH is defined according to ethanol and acetaldehyde, respectively.

Reaction conditions for effect of pH on H_2 generation in Figure 2:

(a) H_2 generation from methanol at different pH values. Conditions: 5.0 mL phosphate buffer containing 400 mM CH_3OH, 500 μM [$Cp^*IrCl(phen)$]Cl, 1 mM NAD^+, 4 mg $Cp^*IrCl_2(ppy)$, 0.5 U ALDH and 30 U ADH at 30 °C.

(b) H_2 generation rate at different pH values in (a).

(c) pH dependent activity of ADH for CH_3OH dehydrogenation. Conditions: 500 μL phosphate buffer containing [NAD^+] = 190 μM, [CH_3OH] = 200 mM, 2.4 U ADH at 25 °C.

(d) pH dependent activity of ALDH for HCHO dehydrogenation. Conditions: 500 μL phosphate buffer containing [NAD^+] = 159 μM, [HCHO] =506 μM, 0.63 U ALDH at 25 °C.

(e) pH dependent activity of Catalyst-1 $Cp^*IrCl_2(ppy)$ for HCOOH dehydrogenation. Conditions: 10 mL reaction solution containing 5 mg Catalyst-1, [HCOOH]+[$HCOO^-$]=2 M at 25 °C.

(f) pH dependent activity of mimic enzyme [$Cp^*IrCl(phen)$]Cl for NADH dehydrogenation. Conditions: 500 μL phosphate buffer containing [NADH] = 480 μM, {[$Cp^*IrCl(phen)$]Cl} =20 μM at 25 °C.

TOF calculation of enzymes (ALDH, ADH) :

The catalytic activity of enzymes (ALDH, ADH) is evaluate by U in this manuscript. And the enzyme supplier (Sigma-Aldrich) provide the specific activity of the enzymes. Its measurement unit is u/mg, which represent purity of the enzymes. The turnover number of the enzymes are relevant to the kinds of substrate and enzyme structure. The substrate of ADH is methanol, and the molecular weight of ADH is 141 kDa, which is a tetramer structure and containing 4 equal subunits (informed by Sigma-Aldrich). The substrate of ALDH is formaldehyde, molecular weight of ALDH is 170000, which

was composed of subunits.[9] We also tried to calculate the TOF of each enzyme, assume the samples of enzymes have high purity. According to the definition of TOF, the TOF of each enzyme is:

TOF = (number of reactions in 1 hour) / (number of enzymes in the solution) (S1)

Then,

$TOF = a \times n/(CV) = a \times upm \times K \times 10^{-6}$ (h^{-1}) (S2)

Where a is the reaction rate of whole reaction in manuscript (μmol h^{-1} $kU_{(ALDH)}^{-1}$), n is the number of moles of enzyme in the whole reaction solution, C is the concentration of enzyme (M), V is the volume of solution, upm is the unit of enzyme per mg protein (U/mg), and K is the molecular weight of enzyme (g/mol). For example, for ALDH in Fig. 1b, a_{ALDH} is 300×10^{-6} mol h^{-1} $kU_{(ALDH)}^{-1}$, n is 0.5×10^{-3} $kU_{(ALDH)}$, C is 2.67×10^{-8} M, and V is 5×10^{-3} L. Therefore, TOF_{ALDH} in Fig. 1b is $300\times10^{-6}\times0.5\times10^{-3}/(2.67\times10^{-8}\times5\times10^{-3})=1120$ h^{-1}.

SI-5. Measure the Activity of $Cp^*IrCl_2(ppy)$ for HCOOH dehydrogenation

Firstly, a one-necked round-bottomed flask (25 mL) containing 10 mL HCOOH solution placed in a water bath under ambient atmosphere. The measurement started as soon as the catalyst was added into the solution. A graduated U-tube filled with water or a 100 mL syringe was connected to the reaction flask to measure the volume of evolved gas from HCOOH dehydrogenation. The volume change was recorded by a digital camera. The temperature for volume measurement was kept at 20 ℃ during the measurements.

The gas generated from the HCOOH dehydrogenation was analyzed by GC-G5 (Beijing Persee General Instrument CO. Ltd). The gas chromatography was assembled with TDX-1column, Porapak Q column, FID, TCD and methanizer, N_2 as carrier gas. **Figure S12a** gave the standard H_2 peak on this GC (black line), and the generating gas from HCOOH dehydrogenation catalyzed by $Cp^*IrCl_2(ppy)$ had same peak location (red line). We determined the H_2 proportion of the mixture was about 51.2%, which mean the HCOOH decomposed in a designed pathway, HCOOH➔H_2+CO_2. The CO was detected by FID of the GC. The standard 10 ppm CO was prepared by diluting the 99.995% CO with N_2. The detection limit of CO was below 1 ppm.

The TOF calculation here was based on the number of Ir atoms in catalyst. The calculation equation was[10]

$$TOF = \frac{P_{atm} V_{gas}}{2 n_{Ir} t R T} \qquad \text{(S3)}$$

Where P_{atm} was the atmospheric pressure (101325 Pa), V_{gas} was the gas volume (CO_2+H_2), n_{Ir} was the total mole number of Ir atoms in catalyst in reaction, t was the period for measurement, R was the universal gas constant (8.314 m^3 Pa mol^{-1} K^{-1}), and T (293 K) was the temperature for gas volume measurement (not the reaction temperature).

SI-6. Activity of ADH and ALDH measured by UV-Vis

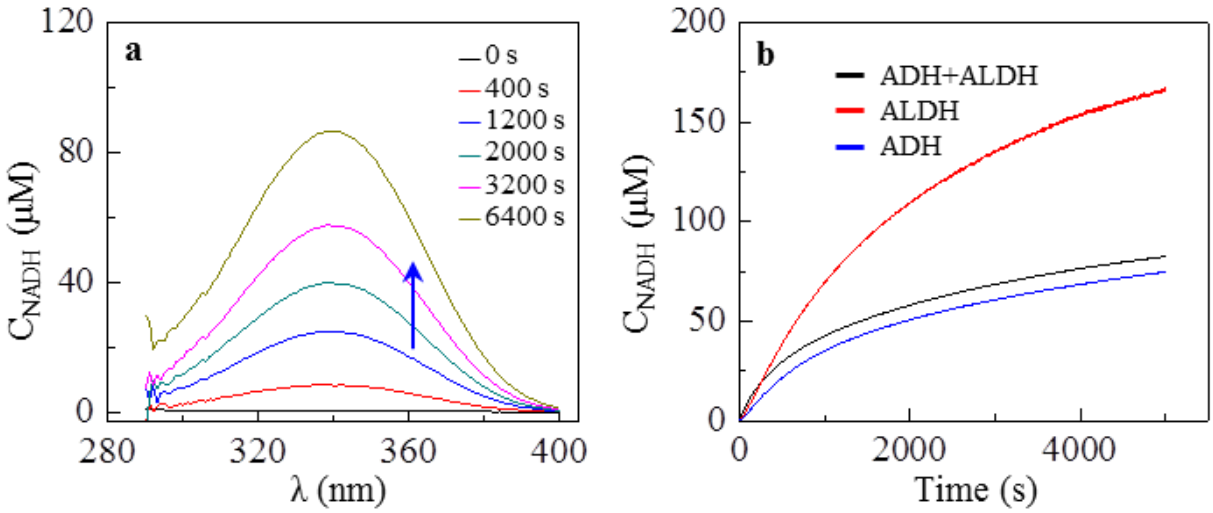

Figure S8. Activity of ADH and ALDH measured by UV-Vis. (a) UV-Vis absorbance spectra of NADH (340 nm) increases with time indicating the methanol dehydrogenation. Conditions: 5U ADH, 500 μM NAD^+, 300 mM CH_3OH, 500 μL phosphate buffer (pH 7.75). (b) NADH concentration versus time trajectory during methanol and formaldehyde dehydrogenation. Conditions: All reactions carried out in 500 μL phosphate buffer at 25℃.

Black curve: 300 mM CH_3OH, 15 U ADH and 0.625 U ALDH, [NAD^+]=200 μM, pH=8.4. Initial reaction rate is 435 μM h^{-1}.

Blue curve: 300 mM CH_3OH, 15 U ADH, [NAD^+]=200 μM, pH=8.4. Initial reaction rate is 165 μM h^{-1}.

Red curve: 506 μM HCHO, 0.625 U ALDH, [NAD^+] = 159 μM. Initial reaction rate is 217 μM h^{-1}.

As the ADH could catalyze CH_3OH dehydrogenation and generating NADH, which would lead to absorbance change at 340 nm on UV-Vis spectrophotometer, accordingly we determined the reaction rate by recording the UV-absorption at 340 nm. The unit of ADH and ALDH is for ethanol and aldehyde, respectively.

SI-7. Characterization of $Cp^*IrCl_2(ppy)$

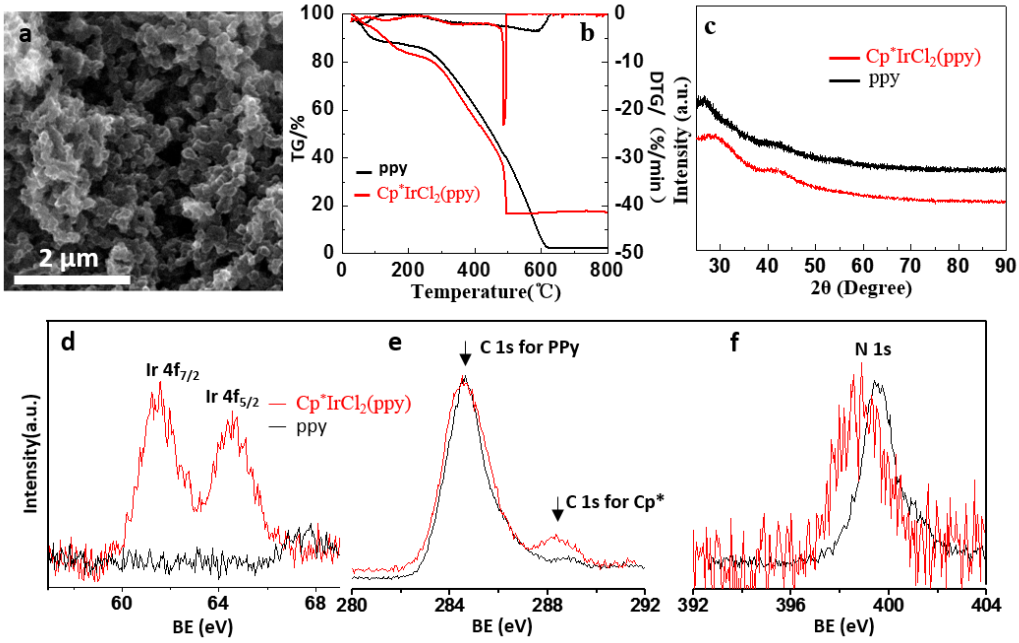

Figure S9. Characterization of catalyst. (a) SEM image of ppy. (b) TG and DTG patterns of ppy and $Cp^*IrCl_2(ppy)$. (c) XRD pattern of ppy and $Cp^*IrCl_2(ppy)$. (d-e) XPS spectra of ppy and $Cp^*IrCl_2(ppy)$.

Recently, a great progress has been achieved in both homogenous and heterogeneous catalysts for formic acid dehydrogenation.[11, 12, 13, 15, 25, 26] Usually, homogenous catalysts show higher activity and selectivity than heterogeneous ones at room temperature.[10, 11] But homogenous catalysts are hard to be separated from the reaction system. In order to synthesize a catalyst with the advantages from both homogenous and heterogeneous catalysts, we use polymer ppy to synthesize a new polymer complex catalyst $Cp^*IrCl_2(ppy)$ (Figure S9). This catalyst can work at very low concentration of HCOOH (5 mM) at near-room temperature (Figure S13a). Figure S13b shows that the selectivity of this catalyst is also high (undetectable CO, << 10 ppm).

Figure S9a showed a typical SEM image of ppy, the polymer chain was agglomerated, the size of most particles was more than 100 nm, also had a porous structure and large surface area. The porous structure would provide a chemical access for high-efficiency mass transfer during the HCOOH dehydrogenation.

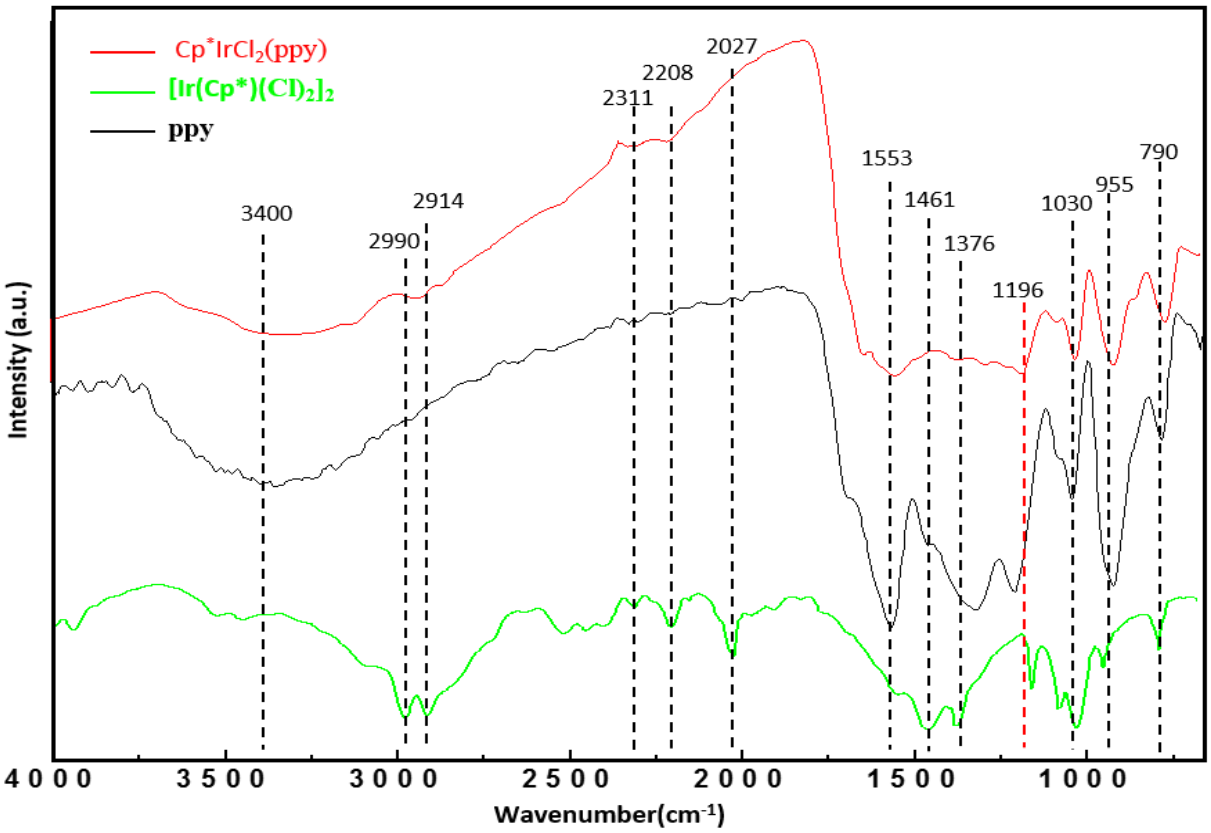

Figure S10. Infrared spectra of ppy, $[Ir(Cp^*)(Cl_2)]_2$ and $Cp^*IrCl_2(ppy)$. Infrared Spectroscopy was detected by Nicolet iN10 (Nicolet Instrument Co. USA). The catalyst power was dispersed on the gold plate, and then the IR data was collected directly by the Nicolet iN10.

A broad peak of around 3400 cm^{-1} could correspond to N–H stretching vibrations of ppy structure in $Cp^*IrCl_2(ppy)$. The weak peaks at 2914 cm^{-1} and 2990 cm^{-1} are attributed to C-H stretching vibration of $-CH_3$ and $-CH_2=CH_2-$ in Cp* of the catalyst. The weak peaks at 2311 cm^{-1} and 2208 cm^{-1} could be attributed to Cp* of the catalyst. The weak peaks at 1553 and 1461 cm^{-1} could correspond to the C=C and C–C stretching vibration in the pyrrole ring of catalyst. The absorption peaks at 1376–790 cm^{-1} are associated with C–N stretching vibrations, in-plane C–H bending vibrations, out-of-plane C–H bending vibrations and N–H deformations, respectively. The characteristic peaks of ppy structure in catalyst are similar to these peaks in literature.[13-15]

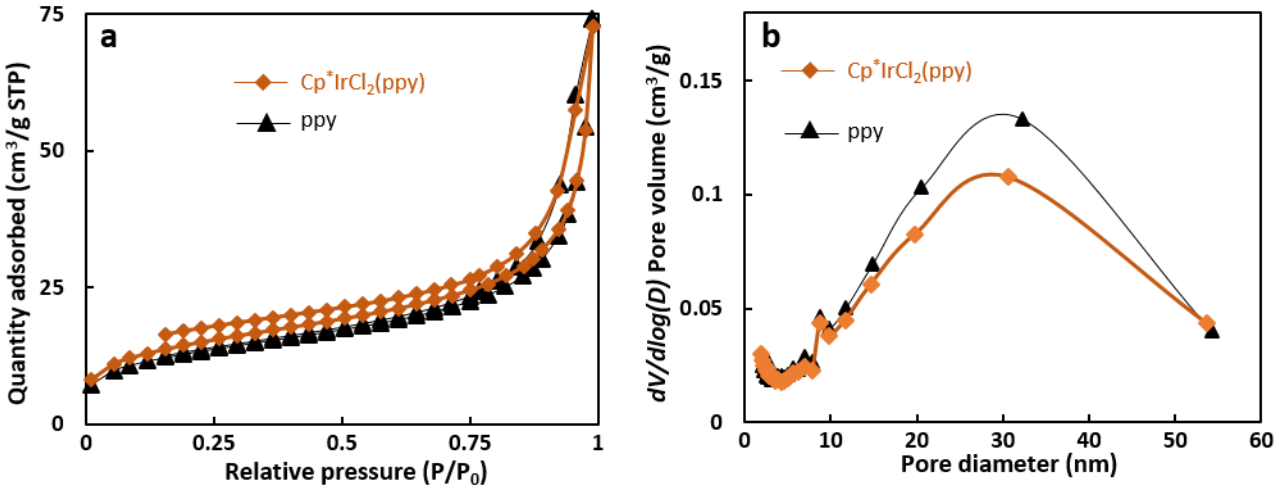

Figure S11. Surface area and pore size analysis (a) N_2 BET adsorption/desorption isotherms for the ppy and Cp^*IrCl_2(ppy) catalyst, black line for ppy and red line for Cp^*IrCl_2(ppy). (b) BJH pore size distribution of the same samples in a.

Both ppy and catalyst have big specific surface area and porous structure (Figure S11), so the N_2 BET adsorption/ desorption was carried out for them. The result proves the ppy and Cp^*IrCl_2(ppy) both have a big specific surface area, 45.5 $m^2\ g^{-1}$ and 51.0 $m^2\ g^{-1}$ respectively (Figure S11a). There are two reasons account for Cp^*IrCl_2(ppy) owning bigger specific surface area. Firstly, the surface of ppy reacting with $[Ir(Cp^*)(Cl)_2]_2$ leads to more complicate surface of ppy. Secondly, although the ppy was insoluble in DMF at room temperature, the surface of ppy was partly dissolving in DMF during synthesizing the catalyst. The first reason also result in the smaller pore size of Cp^*IrCl_2(ppy) compared with ppy (Figure S11b). The average pore size of ppy is 12.8 nm while the Cp^*IrCl_2(ppy) is 11.4 nm. The Cp^*Ir group binding on the wall of pore in ppy would be responsible for the smaller pore.

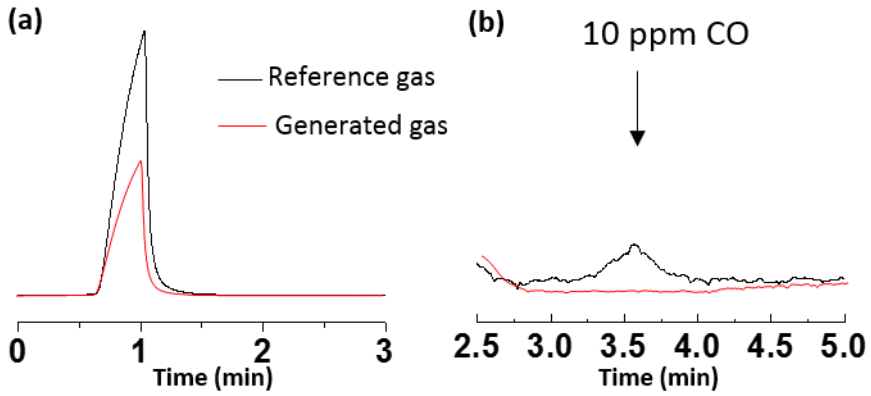

Figure S12. Gas chromatogram of generated gas and reference gas using a TCD and FID detectors. (a) reference (H_2) and generated gas by $Cp^*IrCl_2(ppy)$. (b) Reference (10 ppm CO) and generated gas (black line for reference gas and red line for generated gas).

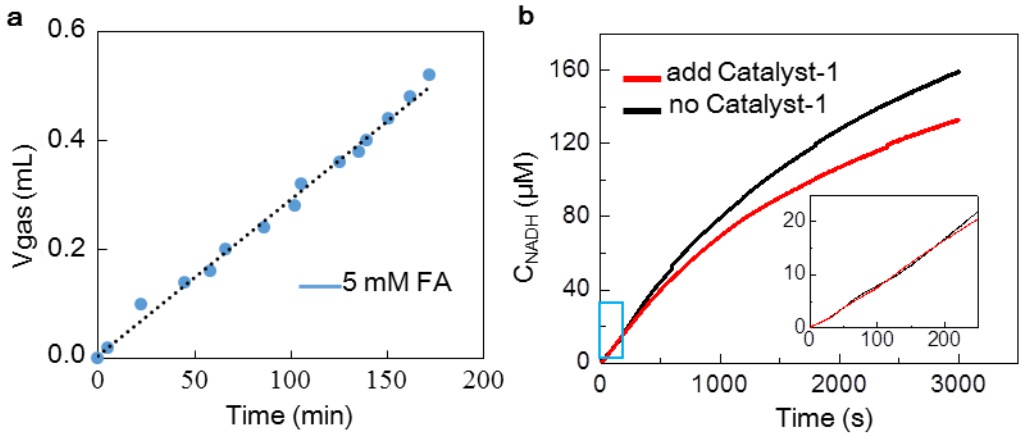

Figure S13. Activity and compatibility of $Cp^*IrCl_2(ppy)$. (a) Evolved gas volume versus time in 5 mM HCOOH containing 10 mM HCHO, 10 U ADH, 1 U ALDH, 1 mM NADH, 5 mM NAD^+, and 50 μM mercaptosuccinic acid. The reaction was performed with 5 mg Catalyst-1 at 30 ℃. (b) The NADH concentration versus time trajectory during methanol dehydrogenation catalyzed by ADH and ALDH. Red line conditions: [CH_3OH] =300 mM, [NAD^+] = 1 mM, {[$Cp^*IrCl(phen)$]Cl} =40 μM, 12 U ADH and 0.2 U ALDH. Black line conditions: [CH_3OH] =300 mM, [NAD^+] = 1 mM, 12 U ADH and 0.2 U ALDH. All reactions carried out in 500 μL phosphate buffer (pH=9) at 25 ℃.

SI-8. Activity of biomimetic hydrogenases on NADH dehydrogenation

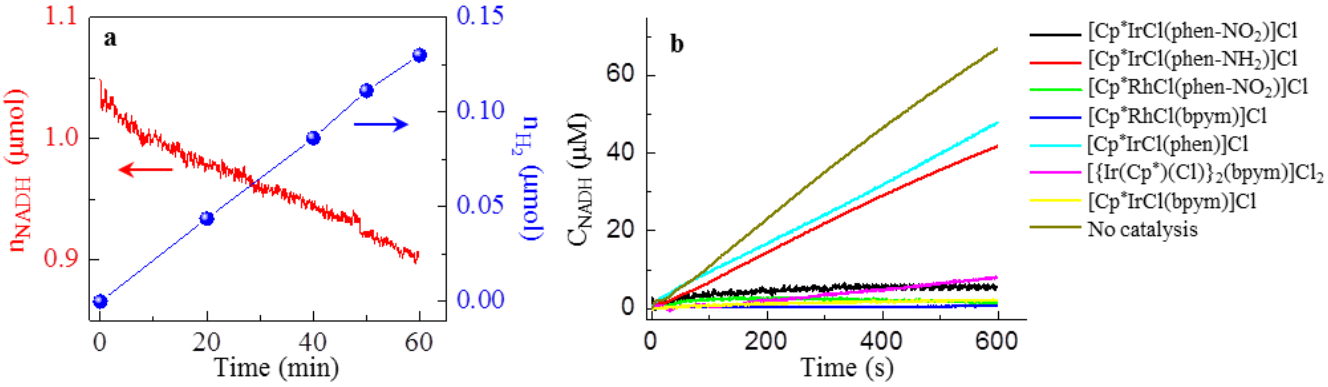

Figure S14. Activity and compatibility of mimic hydrogenases. (a) H_2 generation from dehydrogenation of NADH to NAD^+ by [Cp^*IrCl(phen)]Cl. Condition: [NADH]=420 μM, 2.5 mL phosphate buffer (pH=7.5). (b) Effect of three different mimic enzymes on the activity of ADH. Conditions: [NAD^+] = 1 mM, [CH_3OH] = 300 mM, [catalyst]=30 μM, reactions carried out in 500 μL phosphate buffer (pH=9.0) contain 16 U ADH at 25 ℃. We made the ADH solution mix with 30 μM biomimetic catalyst for 12 hours, then taken the mixed solution for CH_3OH dehydrogenation reaction.

SI-9. Possible mechanism of hydrogen generation from formate and NADH

The catalysts owning the $IrCp^*$ group have the similar catalytic mechanism for formic acid decomposition. So we also propose the possible mechanism according to the literatures.[16-19] A possible reaction mechanism was proposed in Figure S15. The catalytic cycle starts from the Cp^*IrCl_2(ppy) coordinating with water in the formic acid (FA) aqueous solution, forming the intermediate product B (step I). Then the ionized $HCOO^-$ of FA aqueous solution coordinated to B, forms the complex C (step II). After the release of CO_2, we will get the iridium hydride complex D (step III). At last, the iridium hydride D reacts with the H^+ in solution, and produces H_2 and complex B (step IV). This catalytic mechanism is similar with our recent work.[20]

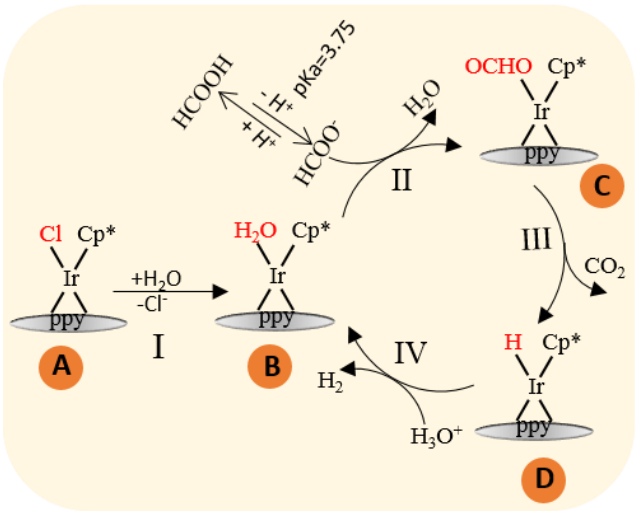

Figure S15. Proposed mechanism for FA dehydrogenation in water.

J. Vijaya Sundar and V. Subramanian have studied the mechanism of hydrogen generation from NADH by water-soluble biomimetic catalyst containing $IrCp^*$ group.[21] We agree with this mechanism, and and propose the similar mechanism for NADH dehydrogenation for our catalyst (Figure S16). Firstly, nicotinamide group of NADH touches the Ir^{3+} ion of $[Cp^*IrCl(phen)]Cl$. Then the H atom transfer from nicotinamide group to the $[Cp^*IrCl(phen)]Cl$, forms the iridium hydride complex and NAD^+. At last, the iridium hydride complex react with the H^+ in solution, and generate hydrogen and $[Cp^*IrCl(phen)]Cl$. The total catalytic cycle finished.

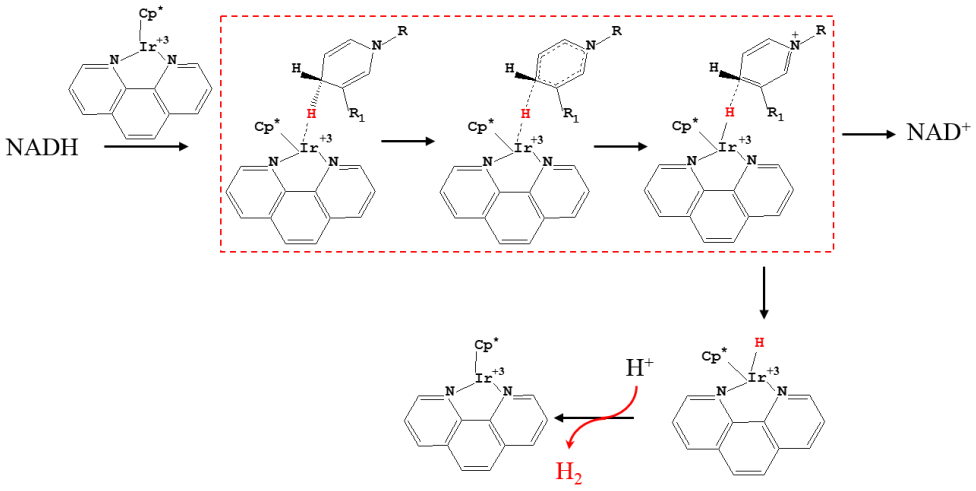

Figure S16. Proposed mechanism for NADH dehydrogenation in water.

SI-10. References

1 S. Machida, S. Miyata and A. Techagumpuch, *Synthetic Metals*, 1989, **31**, 311-318.

2 S. Fukuzumi, T. Kobayashi and T. Suenobu, *Journal of the American Chemical Society*, 2010, **132**, 1496-1497.

3 C. White, A. Yates, P. M. Maitlis and D. M. Heinekey, *Inorganic Syntheses*, 1992, **29**, 228-234.

4 P. Govindaswamy, J. Canivet, B. Therrien, G. Süss-Fink, P. Štěpnička and J. Ludvík, *Journal of Organometallic Chemistry*, 2007, **692**, 3664-3675.

5 Z. R. Youinou M T, *Journal of Organometallic Chemistry*, 1989, **363**, 197-208.

6 S. Betanzos‐Lara, Liu, Z., Habtemariam, A., Pizarro, A. M., Qamar, B., & Sadler, P. J, *Angewandte Chemie International Edition*, 2012, **51**, 3897-3900.

7 J. Canivet, G. Süss-Fink and P. Štěpnička, *European Journal of Inorganic Chemistry*, 2007, **2007**, 4736-4742.

8 J. F. Hull, Y. Himeda, W.-H. Wang, B. Hashiguchi, R. Periana, D. J. Szalda, J. T. Muckerman and E. Fujita, *Nature Chemistry*, 2012, **4**, 383-388.

9 N. Tamaki, M. Nakamura, K. Kimura and T. Hama, *The Journal of Biochemistry*, 1977, **82**, 73-79.

10 Q. L. Zhu, N. Tsumori and Q. Xu, *Journal of the American Chemical Society*, 2015, **137**, 11743-11748.

11 J.-M. Yan, Z.-L. Wang, L. Gu, S.-J. Li, H.-L. Wang, W.-T. Zheng and Q. Jiang, *Advanced Energy Materials*, 2015, **5**, 1500107-1500107.

12 K. Jiang, K. Xu, S. Zou and W.-B. Cai, *Journal of the American Chemical Society*, 2014, **136**, 4861-4864.

13 M. Sevilla, P. Valle‐Vigón and A. B. Fuertes, *Advanced Functional Materials*, 2011, **21**, 2781-2787.

14 Y. Mao, Q. Kong, B. Guo, X. Fang, X. Guo, L. Shen, M. Armand, Z. Wang and L. Chen, *Energy & Environmental Science*, 2011, **4**, 3442-3447.

15 J. Huang and Z. Yang, *RSC Advances*, 2015, **5**, 33814-33817.

16 S. Fukuzumi, T. Kobayashi and T. Suenobu, *Journal of the American Chemical Society*, 2010, **132**, 1496-1497.

17 A. V. Bavykina, M. G. Goesten, F. Kapteijn, M. Makkee and J. Gascon, *ChemSusChem*, 2015, **8**, 809-812.

18 J. F. Hull, Y. Himeda, W. H. Wang, B. Hashiguchi, R. Periana, D. J. Szalda, J. T. Muckerman and E. Fujita, *Nature Chemistry*, 2012, **4**, 383-388.

19 Z. Wang, S. M. Lu, J. Li, J. Wang and C. Li, *Chemistry - A European Journal*, 2015, **21**, 12592-12595.

20 Y. Du, Y.-B. Shen, Y.-L. Zhan, F.-D. Ning, L.-M. Yan and X.-C. Zhou, *Chinese Chemical Letters*, 2017, DOI: 10.1016/j.cclet.2017.05.018.

21 J. V. Sundar and V. Subramanian, *Organometallics*, 2012, **31**, 8525-8536.